Continental Shelf Research 224 (2021) 104473

Contents lists available at ScienceDirect

Continental Shelf Research

journal homepage: www.elsevier.com/locate/csr

Waterside convection and stratification control methane spreading in supersaturated Arctic fjords (Spitsbergen)

Ellen Damm [a,*], Ylva Ericson [b,c,d], Eva Falck [b,c]

[a] Alfred-Wegener-Institut Helmholtz-Zentrum für Polar- und Meeresforschung, Bremerhaven, Germany
[b] Department of Arctic Geophysics, University Centre in Svalbard, Longyearbyen, Norway
[c] Geophysical Institute, University of Bergen, Norway
[d] Norwegian Polar Institute, Tromsø, Norway

ARTICLE INFO

Keywords:
Arctic fjord water
Two year time series
Methane spreading and supersaturation
Waterside convection
Water stratification
Seepage activities in spitsbergen

ABSTRACT

Seasonally ice covered in the past, the fjords in West Spitsbergen turn into being perennially ice free in the present. This feedback to Arctic amplification of global warming changes gas fluxes at the atmosphere-ocean interface. Furthermore, in this Polar region, coupled feedbacks likely enhance Arctic amplification of global warming as numerous gas seepages provide evidence for active gas emissions at the sediment-water interface. We present a time series (2015–2017) of dissolved methane concentrations combined with hydrographic data in Adventfjorden and Tempelfjorden, two sub-fjords of Isfjorden located at the west coast of Spitsbergen. While both sub-fjords remained permanently supersaturated, we detected pronounced temporal and spatial variations in the methane excess level. Our study revealed that seasonal water transformations were key to seasonally changing methane pathways including potential sea-air flux (efflux). We suggest that a cascade of feedback processes, seasonally triggered by waterside convection and stratification, adjusts the amount of methane released and transported within fjord water. When sea ice was missing, strong winter cooling affected the methane supersaturation in contrary directions: first a drop and then a strong increase. In early winter, convective mixing favoured efflux, which reduced the supersaturation. Later in winter, the thermal convection resulted in a continuous overturning of the water column. When the thermal convection reached the bottom, sediment resuspension by turbulence increased, which in turn encouraged enhanced methane release. Subsequently transported along vertical isopycnals, methane from the bottom water reached the water-atmosphere interface. These coupled events created a steady state, simultaneously maintaining supersaturation and efflux. During the warm season, the fjord water became stratified and methane transport occurred mainly laterally in the bottom water. The seasonally changing hydrographic conditions strongly triggered the methane spreading in both sub-fjords and point to a switch between the atmosphere and ocean as main sinks in winter and summer, respectively. Upcoming variations in seasonality, i.e. warmer/cooler summer compared to colder/warmer winter will influence these pathways and the final fate of methane discharged into Arctic fjords.

1. Introduction

Sea ice retreat in the Arctic Ocean, observed since 1979, has recently resulted in the annual September minimum sea ice extent being roughly 25% less than the average between 1981 and 2010 (Perovich et al., 2018). In addition to the progressive degradation of multiyear and prevalence of seasonal sea ice in the high Arctic, Polar regions seasonally ice covered in the past are becoming perennially ice free (Parkinson and Cavalieri, 2012; Stroeve et al., 2012). As a feedback to Arctic amplification of global warming, missing sea ice in turn induces intense shifts at the atmosphere-ocean interface, e.g. sea-air gas fluxes. Indeed, sea ice retreat is under discussion to encourage the atmospheric burden of the potent greenhouse gas methane (CH_4), since recent increases in atmospheric methane concentrations in Arctic regions with fractional sea ice cover and in close proximity to open leads are reported (Kort et al., 2012).

Dissolved methane follows a pronounced seasonal dynamic: cooling and waterside convection encourage sea-air flux during the cold season until sea ice forms while water stratification induced by sea ice melt restricts methane release in summer (Damm et al., 2015). Reduced gas

* Corresponding author.
E-mail address: Ellen.Damm@awi.de (E. Damm).

https://doi.org/10.1016/j.csr.2021.104473
Received 17 November 2020; Received in revised form 20 May 2021; Accepted 21 May 2021
Available online 31 May 2021

transfer in the presence of less sea ice cover and a stratified water column has been reported (Rutgers et al., 2014). By comparison, enhanced gas transfer was observed to occur over the winter due to waterside convection (Anderson et al., 2017). Hence, yet unconsidered seasonal impacts of water transformations on methane pathways are likely to be key in understanding the cycle of this greenhouse gas, especially in Polar regions becoming perennially ice free.

The West Spitsbergen fjord systems (Fig. 1) belong to the regions where winter sea ice has substantially decreased over the last decade, both in terms of maximum sea ice cover and days of fast ice (Muckenhuber et al., 2016). The main waterside effect of sea ice formation is brine release which induces haline convection and the formation of dense bottom water, while in comparison thermal convection homogenize the water column in winter when sea ice is missing (Nielsen et al., 2008).

During the short summer season, large freshwater input from glaciers and rivers contributes to a pronounced water stratification in the fjords (e.g. Svendsen et al., 2002; Cottier et al., 2005; Nilsen et al., 2008). Unique for Polar regions, those pronounced seasonal and sea ice depending water transformations might affect methane pathways as observed during a winter Polynya study in Storfjorden (Damm et al., 2007). Affecting the methane source-sink balance in the high latitudes, those cascades of feedbacks strongly point to previously unconsidered marine-air interactions.

The West Spitsbergen slope and shelf, including the fjord systems such as the highly branched Isfjorden (Fig. 1b), are home to large submarine reservoirs of methane. Linked to the deep bedrock sources through fluid-flow systems, hydrocarbons migrate upwards to the seafloor (Mørk et al., 1984; Nøttvedt et al., 1993; Hustoft et al., 2009; Roy et al., 2014). Considering this circumstance, Isfjorden is a key area to trace the burden of submarine methane in the fjord water with regard to varying seasonal pathways. Furthermore, this region is supposed to be relevant in tracing two postulated feedbacks to Arctic amplification, i.e. methane emissions from Polar water to the atmosphere and sea ice retreat.

To test if sea ice retreat in Polar fjords influences methane pathways and the potential for efflux, we carried out a two year time series on selected stations in two sub-fjords of Isfjorden on the West coast of Spitsbergen (Fig. 1). The focus of our study is on the distribution of methane within the water column affected by seasonal variations of the hydrographic conditions. We revealed pronounced seasonal variations in terms of methane spreading, which in turn results in a switch between the atmosphere and ocean as the final sink of the seafloor-released methane.

2. Regional setting

Adventfjorden and Tempelfjorden are two side fjords of Isfjorden (Fig. 1b), the largest fjord system at the western coast of Spitsbergen. Spitsbergen has several fjords along its west coast that are influenced by two external source waters (Fig. 1a). Cold and less saline Arctic Water (ArW, $S < 34.7$), that originates from the Barents Sea, is carried by the Coastal Current (CC; Fig. 1a) that flows northwards on the shelf (e.g. Cottier et al., 2005; Nilsen et al., 2008) and into the fjords. Warm Atlantic Water (AW) with salinities higher than 34.9 flows northwards along the continental slope with the West Spitsbergen Current (WSC, Fig. 1a). This water can be transported onto the shelf and may propagate into the fjords occasionally (Skogseth et al., 2020) depending on the atmospheric circulation and hydrography of the specific fjords (Cottier et al., 2005; Nilsen et al., 2008, 2016). Transformed Atlantic Water (TAW, $34.7 < S < 34.9$) is a mixture of these two water masses that frequently enters the fjords in the deeper layers (Skogseth et al., 2020). Without a sill at the mouth, water is readily exchanged between the central Isfjorden and the outside shelf and slope area. Isfjorden is classified as a broad fjord, which means that the water in the fjord circulates cyclonically along the fjord boundaries, i.e. with inflow in the southern part and outflow in the northern part of the mouth of the fjord (Nilsen et al., 2008; Skogseth et al., 2020).

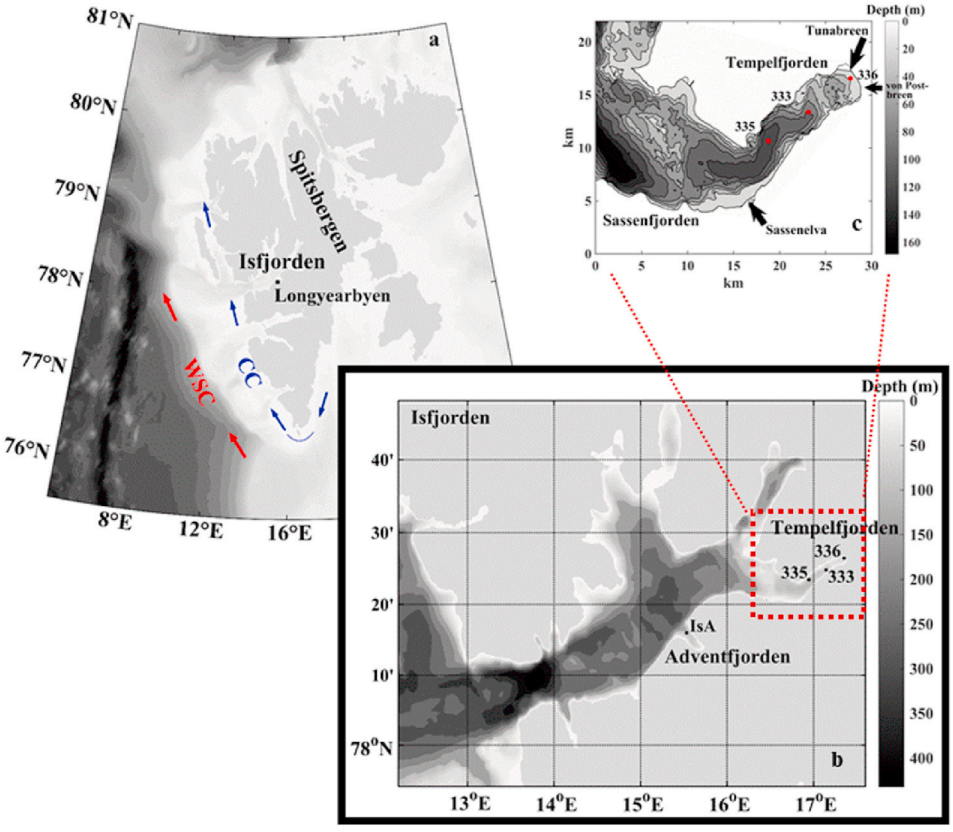

Fig. 1. (a) Map of Spitsbergen with the Coastal Current (CC, blue arrows) and the West Spitsbergen Current (WSC, red arrows). (b) Map of Isfjorden showing the location of the IsA Station (black dot) in Adventfjorden and the Stations 333, 335, and 336 (black dots) in Tempelfjorden. (c) Stations in Tempelfjorden and the glaciers Tunabreen and Von Postbreen (black arrow). (For interpretation of the references to colour in this figure legend, the reader is referred to the Web version of this article.)

Internal processes in Isfjorden during the different seasons produce local water masses (Nilsen et al., 2008; Skogseth et al., 2020). Different types of Winter Water are formed over the dark season. Firstly, dense water is produced due to heat loss to the atmosphere that result in thermal convection (Skogseth et al., 2020). Secondly, for cold winters, sea ice formed and brine is released to the water below, with resultant dense water formation and haline convection (Skogseth et al., 2020). When sea ice is missing thermal convection is dominant (Skogseth et al., 2020). In summer Surface Water is formed as a result of heat transfer from a warmer atmosphere and added freshwater. Sources of freshwater to Isfjorden are either local (precipitation, runoff from land, input of glacial ice (calving), and sea ice melt) or advected into the fjord (freshwater carried by the CC). The formation of Surface Water contributes to a pronounced water stratification during the short summer. Sea ice is formed in the Isfjorden system each winter, but the spatio-temporal extent has decreased (Muckenhuber et al., 2016) and the ice cover in Isfjorden today mainly consists of fast ice formed in the side fjords. Occasionally, drifting sea ice may enter from the shelf region.

Adventfjorden, a small side fjord situated in the southern part of Isfjorden (Fig. 1b), is approximately 50 km from the open coast. The fjord is about 8 km long and 3.5 km wide and less than 100 m deep. Water depths vary mostly from 50 to 80 m in the central part, and only in the fjord mouth, they reach down to nearly 100 m. The wide and deep fjord inlet, without a sill, provides easy water exchange with the central Isfjorden. The outer part of the fjord can also be regarded as a broad fjord, and consequently takes part in the cyclonic circulation of the Isfjorden system (Skogseth et al., 2020). Two rivers supply Adventfjorden with meltwater from snow and nearby land-based glaciers during the summer months. From November to May the rivers in Svalbard are generally frozen. Hence the supply of terrigenous material to the fjords is small (Węsławski et al., 1999). The surface of the fjord used to be ice covered in winter, but during the last decade, sea ice has been scarce in Adventfjorden with no sea ice during the study period.

Tempelfjorden is the easternmost fjord branch of the Isfjorden system (Fig. 1b–c). It is 14 km long and covers an area of 57 km^2 (Forwick et al., 2010). With a width of 5 km, this branch is also wide enough to be affected by rotational dynamics. However, water exchange is to some extent restricted. From central Isfjorden one has to pass Sassenfjorden (Fig. 1c) to get to Tempelfjorden. In Sassenfjorden there is a sill with a maximum depth of about 55 m, which means that waters from Isfjorden can only overflow and exchange with water behind the sill under certain circumstances. Tempelfjorden has two basins (Fig. 1c), one outer and deeper basin (max 110 m) that is shared with the neighbouring Sassenfjorden and one smaller basin at the innermost part of the fjord (Forwick et al., 2010). A sill (at about 25 m depth) separates the outer and inner basin. The tidewater glacier Tunabreen, at the head of the fjord, and the land-terminating glacier Von Postbreen (Fig. 1c), largely influence the freshwater dynamics of the fjord (Forwick et al., 2010). Fast ice usually forms in Tempelfjorden each winter. In spring, sea ice meltwater contributes to the surface water.

3. Data and methods

Measurements of temperature, salinity, and methane concentration were obtained from four different stations during a period of approximately two years, starting in spring 2015. One station was sampled in Adventfjorden (IsA Station, N78°16.0, E15°32.0) from 2 May 2015 to 7 November 2017 and three stations were sampled in Tempelfjorden

Table 1
Overview of data collected.

Dates	CTD	Stations	Bot. depths (m)	Max sampl. depths (m)	No. of samples
27 May 2015	n/a[a]	IsA	90	90	7
24 Jun 2015	SD204	IsA	95	86	6
23 Nov 2015	SBE37	IsA	93	85	8
2 Dec 2015	SBE37	336, 333, 335	51, 76, 104	45, 70, 90	4, 5, 5
9 Dec 2015	SBE37[b]	IsA	96	91	5
29 Jan 2016	SBE37	IsA, 336, 333, 335	97, 47, 72, 104	88, 39, 24, 49	5, 4, 3, 4
19 Feb 2016	SBE19+	IsA, 336[c], 333, 335	94, 47, 70, 105	80, 40, 50, 85	5, 4, 4, 5
4 Mar 2016	SBE19+	IsA, 336, 333, 335	94, 42, 75, 104	84, 33, 65, 98	5, 4, 5, 5
29 Mar 2016	SBE19+	IsA, 333	95, 80	73, 65	5, 5
19 Apr 2016	SBE19+	IsA	96	82	5
28 Apr 2016	SD204[d]	IsA	97	83	8
29 Apr 2016	SBE19+	335	104	91	5
2 May 2016	SBE19+	IsA	96	79	8
3 May 2016	SBE19+	335	104	85	5
20 May 2016	SBE19+	336[e], 333, 335	36, 78, 105	23, 68, 89	3, 5, 5
1 Jun 2016	SBE19+	IsA, 336, 333, 335	94, 49, 83, 104	86, 39, 68, 88	5, 4, 5, 5
20 Jun 2016	SBE19+	IsA, 336, 333, 335	95, 45, 78, 104	82, 30, 65, 81	5, 4, 5, 5
4 Jul 2016	SBE19+	IsA, 336, 333, 335	98, 42, 75, 103	90, 35, 70, 90	5, 4, 5, 5
1 Aug 2016	SBE19+	IsA, 336, 333, 335	92, 46, 82, 99	85, 45,70,87	5, 4, 5, 5
20 Sep 2016	SD204[f]	IsA[f], 336, 333, 335[f]	94, 45, 76, 105	84[f], 41, 70, 84[f]	5, 4, 5, 5
11 Oct 2016	SBE19+	IsA, 336[g], 333, 335	100, 39, 74, 104	89, 35, 71, 90	5, 4, 5, 5
1 Nov 2016	SBE19+	IsA, 333, 335	94, 74, 102	85, 68, 92	5, 5, 5
20 Jul 2017	SBE19+	IsA, 336, 333, 335	96, 40,78, 105	86, 36, 68, 86	5, 4, 5, 5
1 Aug 2017	SBE19+	IsA, 336[h], 333, 335	93, 36, 74, 103	84, 25, 65, 89	5, 3, 5, 5
31 Aug 2017	SBE19+	IsA, 336, 333, 335	95, 40, 78, 105	88, 40, 64, 89	5, 4, 5, 5
30 Sep 2017	SBE9	336[i], 333, 335	40, 72, 101	30, 62, 92	5, 7, 8
2 Oct 2017	SBE9	IsA[j]	73	61	7
7 Nov 2017	n/a[k]	IsA, 336, 333, 335	93, 39, 80, 100	80, 25, 65, 90	5, 3, 5, 5
5 Dec 2017	SBE19+	336, 333, 335	41, 76, 102	25, 65, 90	3, 5, 5

Note. [a]CTD-measurements failed, water sample salinity was measured using a probe, WTW Cond 330i, Germany, temperature was extrapolated from the following sampling occasion. [b]Measurements were conducted 10 December 2015. [c]Position altered to N78°26.0, E17°19.4 due to sea ice. [d]Salinity corrected for an offset of −0.10. [e]Position altered to N78°25.9, E17°17.9 due to sea ice. [f]Noise in pressure measurements i.e. pressure was modelled, salinity recalculated for the new pressure, and finally, salinity was corrected for an offset of −0.13. [g]Position altered to N78°25.6, E17°15.6 due to glacier ice. [h]Position altered to N78°26.0, E17°17.6 due to glacier ice. [i]Position: N78°26.0, E17°17.5. [j]Position: N78°16.0, E15°31.6. [k]CTD-measurements failed, water sample salinity was measured using a Portasal 8410A salinometer and was calibrated against IAPSO standard sea water, OSIL Environmental Instruments and Systems, batch: P146. Temperature was obtained using interpolation between the measurements of the previous and the following sampling occasions.

(Station 336, N78°26.5, E17°21.2, Station 333, N78°24.8, E17°8.7, and Station 335, N78°23.5, E16°56.7) between 2 December 2015 and 5 December 2017 (Fig. 1b). A small boat was used to get from Longyearbyen (Fig. 1a) to the stations. No samples were taken at the IsA Station in July–Oct 2015 and all stations have unfortunately a gap in the data collection between December 2016 and June 2017 (Table 1) due to motor failure of the boat used.

The IsA Station is located near the entrance of Adventfjorden in roughly 90 m water depth. In total, the station was sampled 24 times during the period May 2015 and November 2017. Station 336 (sampled 17 times) was situated in the inner basin of Tempelfjorden with a water depth of around 50 m, while Station 333 (sampled 19 times) and Station 335 (sampled 20 times) were situated in the outer basin, with water depths of 75 and 105 m, respectively (Fig. 1c). The position of Station 336 varied slightly during the time period due to sea ice or calved glacial ice (Table 1). In winter, sea ice was formed in Tempelfjorden, typically growing outwards from the innermost part of the fjord. In 2016 Station 336 was covered by sea ice already in February and the position of the station was shifted to the ice edge (Table 1). This ice was short lasting, and the more permanent fast sea ice came in mid-March 2016 and covered Station 336 by the end of the same month. The sea ice continued to grow the following month and covered station 333 by the end of April. The sea ice never reached all the way out to Station 335 in 2016. Towards the end of May the sea ice disappeared.

Profiles of salinity and temperature in the water column were obtained using a conductivity–temperature–depth (CTD) system. The principal device used, with few exceptions that are outlined in Table 1, was a Sea-Bird SBE19+ that was calibrated each year. At each CTD station a typical handheld Niskin bottle was used to collect the water samples. A small winch with a meter counter wheel was used when lowering the CTD and the Niskin bottle through the water column. When arriving at the station the CTD with the Niskin bottle mounted on the wire just above the CTD were lowered down to about 5 m above the bottom and the Niskin bottle was closed with a messenger. After this first lowering the Niskin bottle was lowered several times to get all the water samples mentioned in Table 1. Hence, discrete seawater samples for methane concentration were collected in this way at different depths throughout the water column at each CTD station. Water samples were filled bubble free in 120 mL glass vials using *Tygon* tubing, impermeable for gases, and sealed directly with rubber stoppers and crimped with aluminium caps. Duplicate samples for methane concentration were taken at chosen stations.

The samples were stored cold and dark and measured within a few weeks in the lab at Alfred Wegener Institute for Polar and Marine Research (AWI) Bremerhaven, Germany. Before measuring 5 mL of N_2 was added into the vials, and then equilibrated for 1 h at room temperature. Afterwards, 1.5 mL gas sample was taken from the headspace and injected into a gas chromatograph (Agilent GC 7890B) with a flame ionization detector (FID). For gas chromatographic separation a 12 µm molecular sieve 5A column (30 m long, 0.32 mm width) was used. The GC was operated isothermally (60 °C) and the FID was held at 200 °C. A calibration curve was done prior to measuring samples using 4.99, 10.00, 24.97, and 50.09 ppm standard gas mixtures. The standard deviation of duplicate analyses was less than 5%. This overall error is almost exclusively due to the headspace procedure, the GC precision had an error of 1%.

Potential density anomaly (σ_0, i.e. density minus 1000) was calculated from the temperature and salinity data using Ocean Data View (ODV; *Schlitzer, Reiner, Ocean Data View,* https://odv.awi.de*)*. The percent methane saturation relative to atmospheric equilibrium was calculated from the concentration, using the CTD temperature and salinity values at the corresponding sampling depth. Gas solubility was calculated following Wiesenburg and Guinasso (1979) and using the atmospheric mole fraction of the monthly mean from November 2015 to December 2017 (NOAA global sampling networks, sampling station Zeppelin station, Spitsbergen http://www.esrl.noaa.gov). The saturation of methane relative to the atmospheric background is shown in addition to the methane concentration (Figs. 2–5) and will be used in the discussion as a normalized concentration. ODV has been used to visualise the data, and the interpolations between the data points were done by this program using weighted-average gridding. The seasons are related to the months as follows: winter from January to April, spring from May to June, summer from July to September, and autumn from October to December.

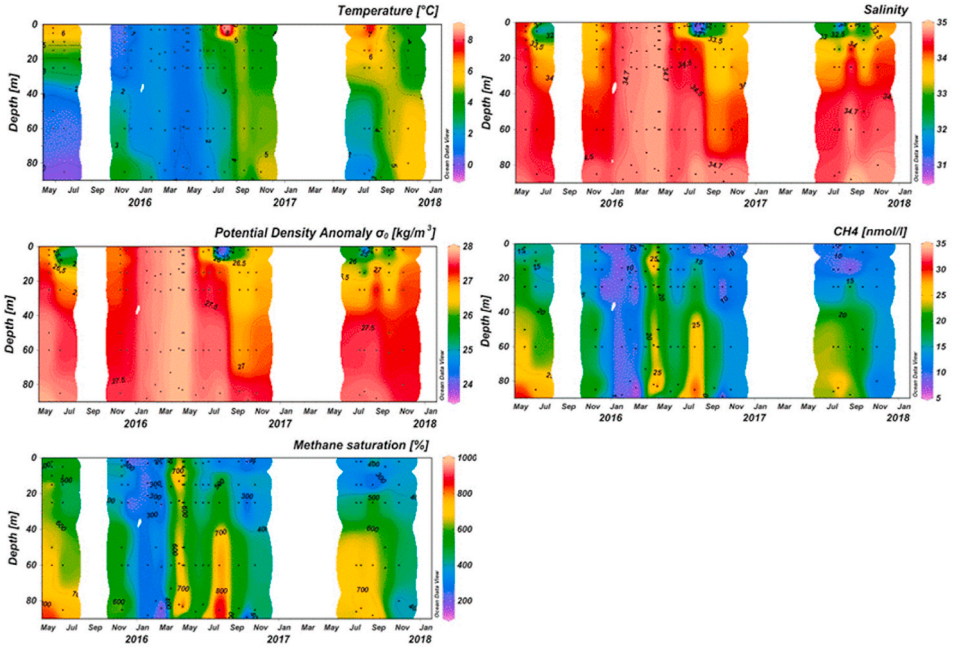

Fig. 2. Time series of temperature, salinity, potential density anomaly, methane concentration, and percent methane saturation at the IsA Station in Adventfjorden from May 2015 to November 2017. White colour shows gaps in the data and black dots show the time and depths of the water sampling. (For interpretation of the references to colour in this figure legend, the reader is referred to the Web version of this article.)

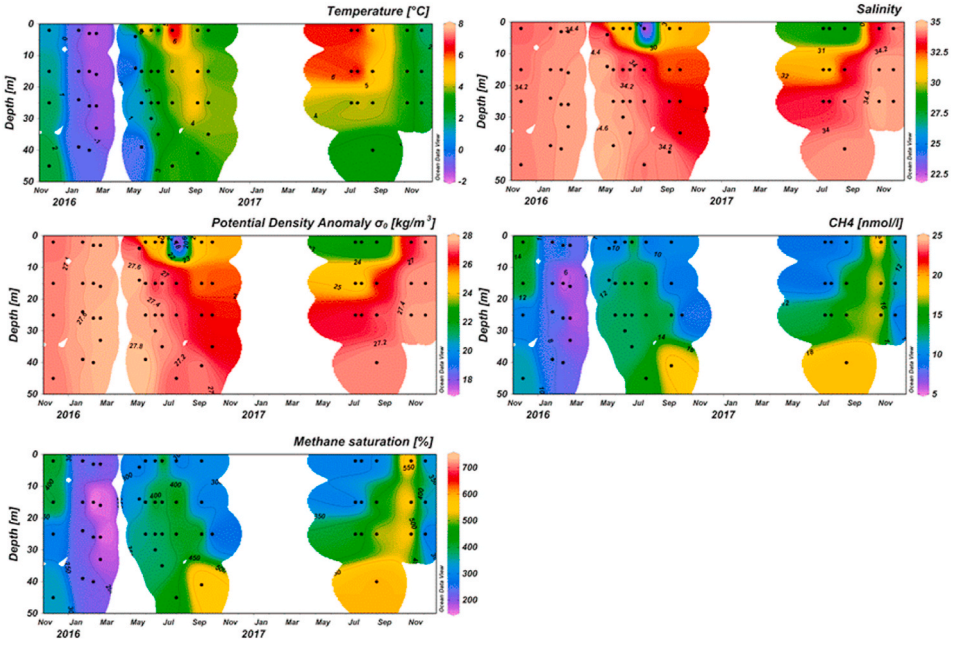

Fig. 3. Time series of temperature, salinity, potential density anomaly, methane concentration, and percent methane saturation in Tempelfjorden at Station 336 from December 2015 to December 2017. White colour shows gaps in data and black dots show the time and depths of the water sampling. Note the different scale for methane concentration and saturation compared to Adventfjorden. (For interpretation of the references to colour in this figure legend, the reader is referred to the Web version of this article.)

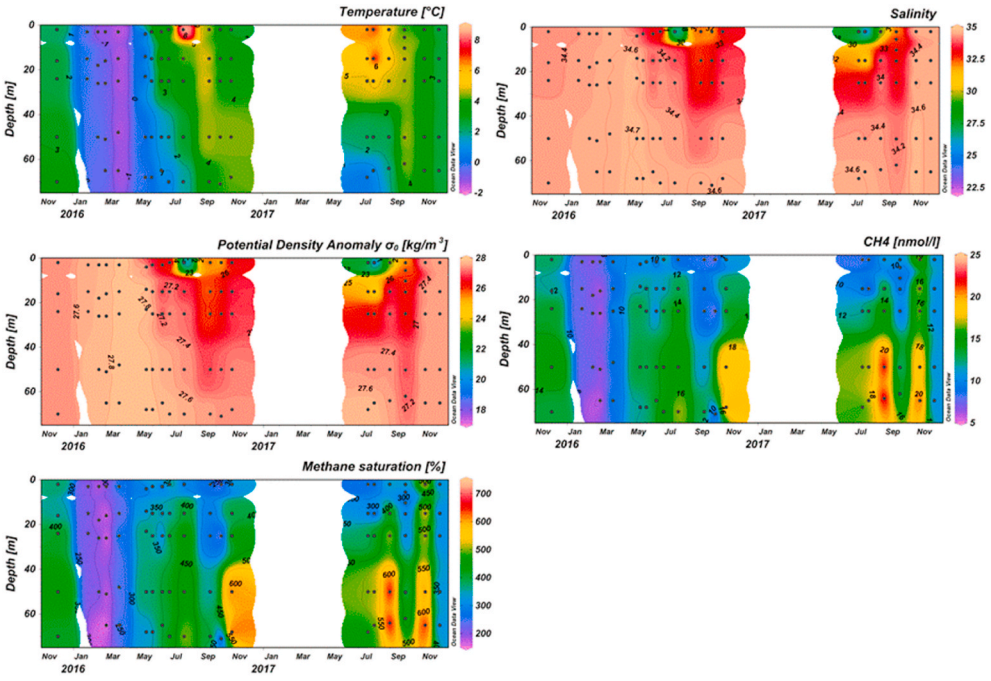

Fig. 4. Time series of temperature, salinity, potential density anomaly, methane concentration, and percent methane saturation in Tempelfjorden at Station 333 from December 2015 to December 2017. White colour shows gaps in data and black dots show the time and depths of the water sampling. Note the different scale for methane concentration and saturation compared to Adventfjorden. (For interpretation of the references to colour in this figure legend, the reader is referred to the Web version of this article.)

4. Results

4.1. Adventfjorden

The time series of temperature, salinity, density, methane concentration, and percent methane saturation for the IsA Station is shown in Fig. 2. The figure shows that the whole water column was well mixed in all properties from January to the beginning of May 2016. The temperature remained well above the freezing point all winter, so no ice formed. The salinities in 2015 and early 2016 were below 34.6 (ArW), but in January 2016 AW entered Isfjorden and reached the IsA Station in February 2016 as TAW ($S > 34.7$, $T > 1\ ^{\circ}C$). During summer, the water column was strongly stratified with surface temperatures reaching 6–8 °C and surface salinities well below 34. For the summers 2016 and 2017, TAW was present close to the bottom at the IsA Station. The methane concentrations varied between 5.8 and 33.5 nM, lowest concentrations were found in January–March 2016 and highest during spring/summer. The saturation concentration for these waters was 3–3.5 nM, so the water was always supersaturated. The percent methane saturation varied between 169% and 974%.

4.2. Tempelfjorden

The time series of temperature, salinity, density, methane concentration, and percent methane saturation for the three stations in Tempelfjorden are presented in Figs. 3–5. In December 2015, the

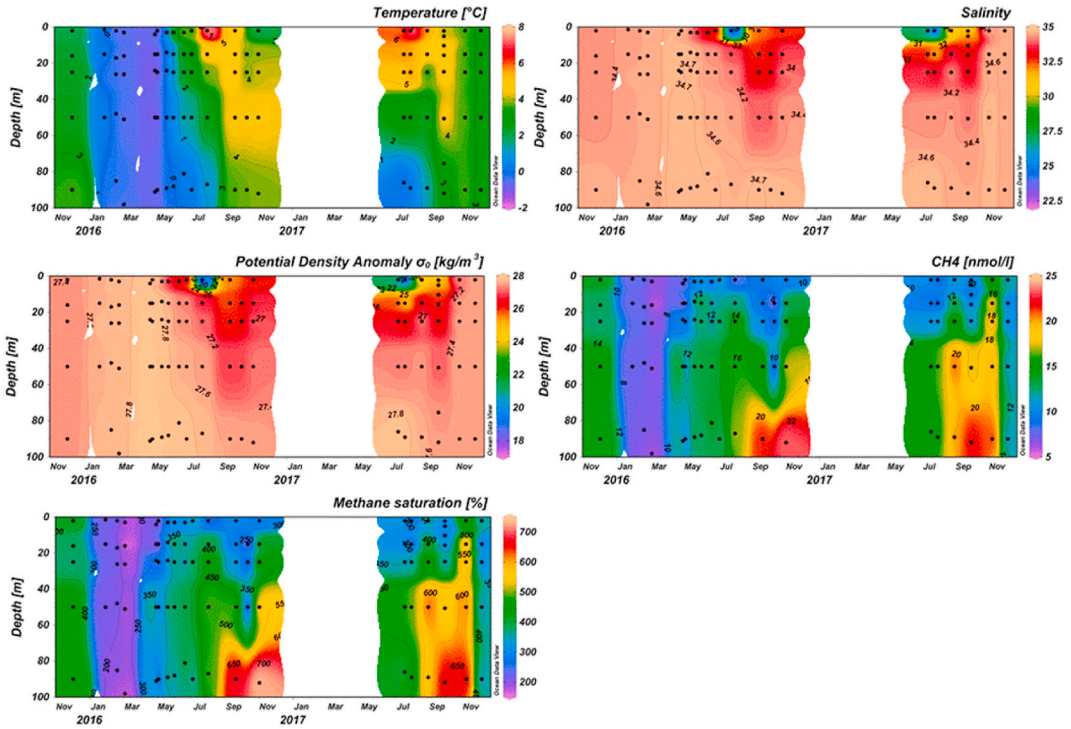

Fig. 5. Time series of temperature, salinity, potential density anomaly, methane concentration, and percent methane saturation in Tempelfjorden at Station 335 from December 2015 to December 2017. White colour shows gaps in data and black dots show the time and depths of the water sampling. Note the different scale for methane concentration and saturation compared to Adventfjorden. (For interpretation of the references to colour in this figure legend, the reader is referred to the Web version of this article.)

temperatures were above 1 °C at all depths at all three stations, these had decreased to values between −0.2 and −1.64 °C by the middle of February 2016. The lowest temperature was observed at the surface at the innermost station (Station 336, Fig. 3). The surface values at that time for the other two stations were −1.33 °C (Station 333, 5″, Fig. 4) and −0.53 °C (Station 335, Fig. 5). Sea ice started to form near the glacier front and by the end of March the fast ice extended all the way out to Station 336. At the end of March 2016 only Station 333 could be taken, the temperature at this station had then decreased to −1.48 °C (Fig. 4). In December 2015, the freshest water with a salinity about 34.0 was found at the surface at Station 336 (Fig. 3). Deeper down in the water column and further out in the fjord the salinity increased to values of up to 34.6. The highest salinity values were measured in April and May, reaching values slightly above 34.7 at Station 333 (Fig. 4) and Station 335 (Fig. 5). In January 2016, the convection had reached the bottom at all three stations and by the end of March, the density anomaly shows that the water column is vertically homogenous. The methane concentration and percent saturation in the water column decreased from about 14 to 5–6 nM and from about 400% to 150–160%, respectively, during this period, and reached the lowest values in March. At the end of April and beginning of May, only Station 335 was sampled, since this station was not covered by sea ice. By the end of May most of the sea ice in the fjord was gone and the stratification of the water column had started.

The observed maxima in temperature and minima in salinity occurred in the surface layer in the beginning of August in both 2016 and 2017. The surface temperature and salinity reached values between 6.8 and 8.7 °C and 22 and 24, respectively, with values in the lower range at Station 336. The highest methane values were found near the bottom in August/September in both years for all three stations, with methane concentration between 19 and 23 nM and methane saturation between 590% and 730%. The lowest values were observed at the innermost station (Station 336) and the highest values at the outermost and deepest station (Station 335). Between September and December, the methane concentration was between 16 and 18 nM in the surface layer and 18–21 nM in the deeper parts. The resulting methane saturation was around 500% in the surface and up to 660% close to the bottom at Station 336. One month later the methane concentrations on all stations had decreased to 10–11 nM, and the methane saturation to around 300%–350%.

5. Discussion

Our two year time series revealed substantially higher methane concentrations relative to the atmospheric equilibrium concentration in Adventfjorden and Tempelfjorden, i.e. both sub-fjords were permanently methane supersaturated. Supersaturation reached nearly 1000% in Adventfjorden and nearly 750% in Tempelfjorden. Further, pronounced vertical gradients clearly indicate methane release at the sediment-water interface. Overall, these features corroborate ongoing methane release at the sediment-water interface, highlight the importance of the water circulation for the methane spreading in the fjord water, and point to internal processes as drivers for the seasonal and spatial variabilities. In general, the methane supersaturation reached maxima in late summer or mid-autumn, dropped in winter down to 200% and started to increase in spring again (Figs. 2–5).

We suggest the following coupled processes as drivers: During late autumn and winter, cooling and subsequent convective mixing homogenized the water column, which in turn initiated methane upward transport along vertical isopycnals. The methane excess was mixed within the water column, and hence a pronounced methane efflux, i.e. water-air flux, took place, eventually reducing the supersaturation in the whole water column. In late spring, water stratification, as a result of surface warming and melt water addition, favoured the formation of methane plumes (i.e. water with high methane concentration) in the bottom water and lateral methane spreading in the fjord system. Hence, in summer and early autumn, long turnover of methane in bottom water encouraged high levels of supersaturation therein. The restricted

vertical transport and continued freshwater discharge into the fjords kept the supersaturation low in the surface water during this time. The cycle closed, when in late autumn, mixing by cooling broke down the water stratification. Then waterside convection balanced the methane excess within the water column before efflux eventually reduced the supersaturation again. These interacting processes describe the general pattern, while local disparities between the observed stations contributed to interannual and seasonal deviations in the source and sink strengths. To highlight the impact of hydrographic processes on methane release at the sediment-water interface and further pathways, we discuss crucial aspects.

5.1. The impact of water stratification in spring and summer

In spring, a well-developed surface layer gradually took form because of warming, sea ice melt, increased glacier melt, and river water inflow. The freshwater discharge resulted in water stratification most pronounced in late summer when maxima in temperature and minima in salinity occurred in the surface layer. This water stratification isolated the deep water from the surface water, and strong vertical gradients in methane concentration are seen at all stations (Figs. 2–5).

Contemporaneously increasing methane concentrations in bottom water corroborate the formation of methane plumes. (Figs. 2–5). The shape of these plumes follow the shape of the density gradients and are most evident from July to August in Adventfjorden and from August to September in Tempelfjorden. This slight temporal shift between both fjords certainly reflects the direct coupling between the build-up of water stratification and the formation of methane plumes in bottom water. Predominantly lateral transport and plume formation encouraged by water stratification have also been reported from the West Spitzbergen shelf region (Damm et al., 2005; Gentz et al., 2014; Silyakova et al., 2020).

During the warm season the supersaturation remained sustained also in the surface water, although on a lower level; in Adventfjorden between 300 and 500% and in Tempelfjorden between 200 and 300% (Figs. 2–5). This permanently sustained supersaturation in the surface water points to mixing of methane from the bottom water plume and/or by methane released from shallower parts of the fjords balancing the efflux, i.e. a steady state is established. The slightly higher supersaturation in summer compared to winter indicates a less effective efflux during the warm season, probably caused by less strong winds. Further, freshwater discharge dilutes the methane excess, i.e. there is no discharge of methane via river and glacier melt water into the fjord.

5.2. The impact of deep convection in autumn and winter

In autumn, wind mixing and cooling eroded the water stratification and the mixed layer depth increased. Contemporaneously, the vertical gradient in methane saturation weakened and the level of saturation decreased from about 800% in the bottom layer at the IsA Station and from a somewhat lower saturation value at the stations in Tempelfjorden, to below 300% in January in the whole water column (Figs. 2–5). In February 2016 fast ice started to form in Tempelfjorden, while in Adventfjorden no ice formed. Remarkably, this circumstance, which results from several important hydrographic differences between the two fjords, contributes to pronounced distinctions to the fate of methane, considered separately in more detail.

5.2.1. Adventfjorden

At the IsA Station, water is readily exchanged with the proper Isfjorden. Inflowing cold ArW dominated from spring 2015 to early winter while in February 2016 the warmer TAW replaced the ArW (Ericson et al., 2018, Skogseth et al., 2020). Hence, the water temperature remained above freezing during the whole winter, with a higher air-sea temperature difference than what was observed in Tempelfjorden. The large temperature gradient between the air and ocean and lack of sea ice formation, resulted in strong cooling of the water column, which induced, an intense convective mixing during the late autumn and the

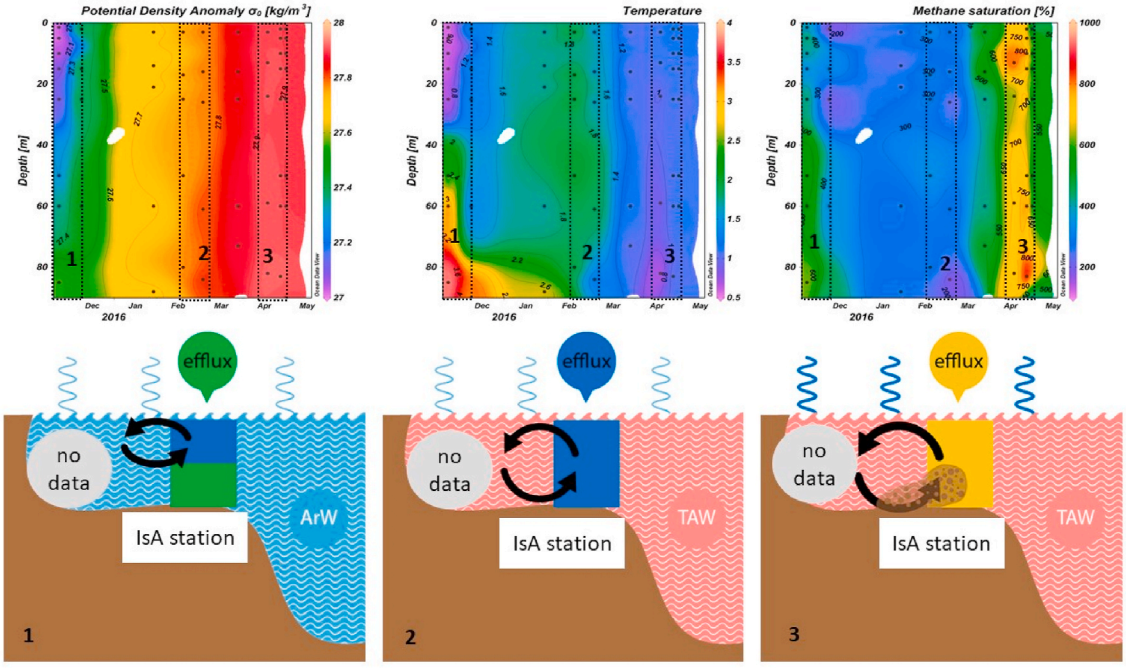

Fig. 6. The change of the potential density anomaly, temperature, and percent methane saturation over time, i.e. from the November 2015 to May 2016 section of the IsA Station time series in Adventfjorden. In early winter 2016 (1) cooling and convection started to homogenize the water column. The methane supersaturation decreased. In late February (2) ArW was replaced by TAW, thermal convection created vertical isopycnals. These coupled processes induce a pronounced drop of the supersaturation until the beginning of March. In late April (3) cooling in the fjord system reinforced the thermal convection and methane saturation contemporaneously started to increase again in the whole water column. This combined pattern indicates methane release at the sediment-water interface and transport along vertical isopycnals to the surface water, i.e. a steady state between the bottom and surface water existed (see text).

whole winter, shown in the density shifts from 27.6 kg m^{-3} in December to nearly 28 kg m^{-3} in late April (Figs. 2 and 6). Revealed by the vertical isopycnals, convective mixing homogenized the whole water column and favoured the efflux which in turn caused a stepwise decrease in the supersaturation from about 400% in December 2015 to 200% at the beginning of March 2016. This lower level of supersaturation remained sustained over several weeks. Between late March and late April the methane supersaturation started to increase again, finally reaching more than 700% across the whole water column in the second part of April 2016. Furthermore, as no weakening of supersaturation in the surface water was observed, methane is supposed to be continuously transported upward during this half month period counterbalancing the efflux or with other words, to keep this high supersaturation in the whole water column sustained, an enhanced methane release at the sediment-water interface is mandatory (Fig. 6).

By the middle of May the water column started to get stratified again and the waterside cooling and convective mixing stopped, hence the upward transport of methane to the surface ceased (Fig. 2).

5.2.2. Tempelfjorden

Situated in the inner, eastern, and consequently colder, part of the Isfjorden system, Tempelfjorden is surrounded by glaciers and affected by calving from Tunabreen. This provides for a colder and fresher environment than what is seen in Adventfjorden (Figs. 2–5). Furthermore, the depth averaged current of 2 cm s^{-1} is about half of the observed current at the IsA station (Skogseth et al., 2020), and the sill in Sassenfjorden restricts the entrance to Tempelfjorden to 55 m water depth. Consequently, the ventilation rate in Tempelfjorden is slower than that in Adventfjorden, and the more isolated water column is less affected by intrusions of warm Atlantic water, e.g. no inflow of TAW in February 2016 (Figs. 2–5). Without the heat from TAW, in combination with the above-mentioned features, the water column in Tempelfjorden was cooled down to freezing temperatures, with resultant thermal convection that reached bottom before fast ice formed in the inner part of the fjord. The fast ice restricted the sampling and there are no measurements of the water column below the ice at Stations 336 and 333 in April 2016.

However, the high methane supersaturation in the whole water column corroborates the ongoing vertical methane transport from the sediment-water interface to surface water (Figs. 3–5) before ice formation. Though, this process was restricted to a much shorter period than what was observed in Adventfjorden, and ceased when ice formed. In addition, the efflux ceased as the level of supersaturation remained sustained by about 200% until spring when the ice disappeared and the water column started to get stratified again. This feature likely reflects that the current is especially low in late winter, because of the ice cover and its dampening effect on the wind driven circulation (Skogseth et al., 2020), which also restricts the gas transfer velocity. The slower current and restricted thermal convection also limit the transport of methane from the sediments to the water column in the open water part of Tempelfjorden. Note that haline convection might have occurred under the ice, but with no data it is not possible to elucidate its potential importance on the methane distribution in the inner part of Tempelfjorden.

5.3. The steady state mode

Remarkable is that during the two years of measurements the methane concentration in both fjords never reached the saturation level corresponding to the equilibrated concentration with the atmosphere. These circumstances point to a steady state mode between the methane source and sink. To keep the supersaturation on a level of more than 200% or higher in all seasons, potential efflux at the water surface and/or lateral transport within the fjord water needs to be balanced by a permanently ongoing methane release at the sediment-water interface.

Current methane release might be encouraged by more or less permanent sediment resuspension induced by sliding friction at the water-sediment interface, generated by changes in the current speed and direction of the bottom water as a consequence of, for instance, the changing tides.

Further, comparing the conditions in both fjords clearly reveal the sea ice effect for the setup of a higher levelled steady state in winter when strong cooling occurs but no sea ice is formed. In shallow ice-free fjords the thermal convection and overturning of the water column favour the formation of a lift system, i.e. direct transport from the sediment-water interface to surface water where efflux occurs. By comparison, the steady state remained kept on the lower level when ice restricts thermal convection and vertical transport.

5.4. Waterside effects on seepage activities

Numerous studies have investigated methane sources in Isfjorden. High accumulation rates of organic matter in Polar fjords (between 5 and 17 g m^{-2} yr^{-1}; Winkelmann and Knies, 2005) favours the microbial formation of methane by degradation of organic matter in near surface sediments. In addition to recently produced methane also fossil methane is likely to reach the fjord water. Linked to upper sediments by subsurface fluid flow systems, methane migrates upwards from deep bedrocks and shallow gas occurrence eventually favours gas seeping into the marine environment (Judd and Hovland 2007; Forwick et al., 2009; Roy et al., 2015 and references therein). Well-known features for abrupt gas discharge are pockmark depressions in sediments, which are widespread in the whole Isfjorden system. These gas seeping activities take place as pressure releases from over-pressured instable sediment layers (Judd and Hovland 2007). Obviously, active in the past the current activity of pockmarks is uncertain and alternatively slow and steady degassing is under discussion as well (Roy et al., 2015; Liira et al., 2019). Additionally, steep methane concentration gradients in sediment cores taken at the entrance to Adventfjorden have been reported by Liira et al. (2019) which would strengthen the release of methane from the sediments. Indeed, frequent resuspension and redeposition events during winter are corroborated by both the granulometric composition of the surface sediments and the high fluxes of redeposited particulate organic carbon in Adventfjorden (Zajaczkowski et al., 2010).

Even though searching for where in the fjord the methane is released from the sediments was outside the scope of our study, our two year time series contribute to highlight the recently ongoing kind of seepage activity. Evidently, we observed a remarkable pattern in methane spreading, strongly linked to the seasonally changing hydrographic conditions (Figs. 2–6). Hence, based on our observations we argue for a slow and steady methane release at the sediment-water interface and hydrographic processes as dynamic control for methane spreading, forming the methane plumes in the water column. By comparison, short-time events of pulsed methane release are expected to create methane plumes in the water column unrelated to seasonal variations in water circulation, i.e. an inconsistency of the methane plume shape with the shape of the isopycnals. Both circumstances in context, point to slow and steady degassing as the dominant recently ongoing seepage activity.

6. Summary and conclusions

The permanent supersaturaton of both fjords clearly indicates an ongoing slow methane release at the sediment-water interface, while variations in supersaturation are affected by varying hydrographic conditions. Based on our data, we postulate that the pronounced seasonality in hydrographic processes acts as one of the key drivers with regard to the type of methane spreading in the fjord water.

During the warm season (May–September) Isfjorden is stratified and sub-marine methane is mainly laterally transported within the bottom water current. The counter-clockwise circulation along the fjord boundaries eventually transports the methane-charged fjord water to the fjord mouth where it is discharged into and mixed with the shelf

water. Although during that journey, methane oxidation might take place to a certain amount (Mau et al., 2013), mixing and dilution in deep shelf water and further transport along the slope further north will be the most likely pathway. Hence, during spring and summer the ocean acts as the main final sink for fjord-sourced methane. Warmer summers with more meltwater discharge to the fjords will reinforce stratification and lateral transport of methane within the densest fjord water.

In winter, we observed potential interactions between the presence or absence of sea ice in the fjords and the amount of methane vertically transported from the sediment-water interface to the water-atmosphere interface. Missing sea ice favours thermal convection down to the bottom and enhances methane release induced by turbulence and sediment resuspension.

Accordingly, the atmosphere might act as the final sink as long as thermal convection continues down to the sediment–water boundary layer. When sea ice covers the fjord the upward methane transport to the atmosphere is interrupted. We recommend flux measurements to validate our assumptions.

Consequently the atmosphere and ocean act as main sinks in winter and summer, respectively, while the switch between both is expected to be strongly coupled to the temperature differences between the seasons, i.e. more distinct between warm summer and cold winter and less pronounced between cooler summer and warmer winter.

Further the shift from seasonally ice covered in the past to recently perennially ice free influences the final fate of methane in Isfjorden.

We hypothesize that vertical methane transport might be kept going when the hydrostatic pressure in the surface sediments is affected by the continuously overturning of the water column. We recommend hydroacoustic measurements to validate potential hydrostatic pressure reduction in the surface sediments affected by hydrographic processes.

This assumption is in accordance with Roy et al. (2015 and 2016). They described pockmarks as features of hydrostatic pressure reduction at the sediment surface and the formation as being active in the past while mostly inactive in the present. Hence, we suggest, to prove the proposed interaction between sea ice cover and pockmark activities by comparing methane pathways in winter in ice-covered and ice-free fjords.

Author contributions

ED and YE designed the study. ED analysed the methane samples and wrote the geochemical part of the manuscript. YE collected the oceanographic data and the methane samples. YE and EF analysed the physical oceanography data and wrote the oceanographic part of the manuscript.

Funding

This study was funded by the PACES (Polar Regions and Coasts in the Changing Earth System) Program of the Helmholtz Association, Germany. The fieldwork was funded by the Norwegian Research Council under the Arctic Field Grant (Research in Svalbard Database nos. 10127; 10404; 10662), with additional support from the University Centre in Svalbard. The study/salary for YE was partly funded by the Flagship research program "Ocean Acidification and effects in northern waters" within the FRAM- High North Research Centre for Climate and the Environment at the Norwegian Polar Institute, Norway.

Data availability

Data will be made available on request.

Declaration of competing interest

The authors declare that they have no known competing financial interests or personal relationships that could have appeared to influence the work reported in this paper.

Acknowledgments

We would like to thank Ilsetraut Stölting for support analysing the methane samples. We also thank the Tech and Logistics department at the University Centre in Svalbard for assistance with the fieldwork.

References

Andersson, A., Falck, E., Sjöblom, A., Kljun, N., Sahlée, E., Omar, A.M., Rutgersson, A., 2017. Air-sea gas transfer in high Arctic fjords. Geophys. Res. Lett. 44, 2519–2526, 10.102/GL2016072373.

Cottier, F.R., Tverberg, V., Inall, M.E., Svendsen, H., Nilsen, F., Griffiths, C., 2005. Water mass modification in an Arctic fjord through cross shelf exchange: the seasonal hydrography of Kongsfjorden, Svalbard, 10. J. Geophys. Res. 110, C12005, 1029/2004JC002757.

Damm, E., Rudels, B., Schauer, U., Mau, S., Dieckmann, G., 2015. Methane excess in Arctic surface water- triggered by sea ice formation and melting. Sci. Rep. https://doi.org/10.1038/srep16179.

Damm, E., Schauer, U., Rudels, B., Hass, C., 2007. Excess of bottom-released methane in an Arctic shelf sea polynya in winter. Continent. Shelf Res. 27, 1692–1701.

Damm, E., Mackensen, A., Budeus, G., Faber, E., Hanfland, C., 2005. Pathways of methane in seawater: plume spreading in an Arctic shelf environment (SW Spitsbergen). Continent. Shelf Res. 25 (12–13), 1433–1452.

Ericson, Y., Falck, E., Chierici, M., Fransson, A., Kristiansen, S., Platt, S.M., Hermansen, O., Myhre, C.L., 2018. Temporal variability in surface water pCO_2 in Adventfjorden (West Spitsbergen) with emphasis on physical and biogeochemical drivers. J. Geophys. Res. Oceans 123. https://doi.org/10.1029/2018JC014073.

Forwick, M., Baeten, N.J., Vorren, T.O., 2009. Pockmarks in spitsbergen fjords. Nor. J. Geol. 89, 65–77.

Forwick, M., Vorren, T.O., Hald, M., Korsun, S., Roh, Y., Vogt, C., Kyu-Cheul, Y., 2010. Spatial and temporal influence of glaciers and rivers on the sedimentary environment in Sassenfjorden and Tempelfjorden, Spitsbergen. In: Howe, J.A., Austin, W.E.N., Forwick, M., Paetzel, M. (Eds.), Fjord Systems and Archives. Geol. Soc., London, Spec. Publ., vol. 344, pp. 163–193. https://doi.org/10.1144/SP344.13.0305-8719/10/$15.00.

Gentz, T., Damm, E., Schneider, v, Deimling, J., Mau, S., McGinnis, D.F., Schlüter, M., 2014. A water column study of methane around gas flares located at the West Spitsbergen continental margins. Continent. Shelf Res. 72, 107–118.

Hustoft, S., Bünz, S., Mienert, J., Chand, S., 2009. Gas hydrate reservoir and active methane-venting province in sediments on <20 Ma young oceanic crust in the Fram Strait, offshore NW-Svalbard. Earth Planet Sci. Lett. 284, 12–24.

Judd, A.G., Hovland, M., 2007. Seabed Fluid Flow. The Impact on Geology, Biology, and the Marine Environment. Cambridge University Press, Cambridge. ISBN-13: 978052181950 3$4).

Kort, S.C., Wofsy, S.C., Daube, B.C., Diao, M., Elkins, J.W., Gao, R.S., Hintsa, E.J., Hurst, D.F., Jimenze, R., Moore, J.R., Spackmann, J.R., Zondlo, M.A., 2012. Atmospheric observation of Arctic Ocean methane emissions up to 82° north. Nature geosc 5, 318–321.

Liira, M., Noormets, R., Sepp, H., Kekišev, O., Maddison, M., Olaussen, S., 2019. Sediment geochemical study of hydrocarbon seeps in Isfjorden and Mohnbukta: a comparison between western and eastern Spitsbergen, Svalbard. Arktos 5, 49–62. https://doi.org/10.1007/s41063-019-00067-7.

Mau, S., Blees, J., Helmke, E., Niemann, H., Damm, E., 2013. Vertical distribution of methane oxidation and methanotrophic response to elevated methane concentrations in stratified waters of the Arctic fjord Storfjorden (Svalbard, Norway). Biogeosciences 10, 6267–6278.

Mørk, A., Bjorøy, M., 1984. Mesozoic source rocks on Svalbard. In: Spencer, A.M. (Ed.), Petroleum Geology of the North European Margin. Springer Netherlands, pp. 371–382.

Muckenhuber, S., Nilsen, F., Korosov, A., Sandven, S., 2016. Sea ice cover in Isfjorden and Hornsund, Svalbard (2000-2014) from remote sensing data. Cryosphere 10 (1), 149–158. https://doi.org/10.5194/tc-10-149-2016.

Nilsen, F., Cottier, F., Skogseth, R., Mattsson, S., 2008. Fjord-shelf exchanges controlled by ice and brine production: the interannual variation of Atlantic Water in Isfjorden, Svalbard. Continent. Shelf Res. 28 (14), 1838–1853. https://doi.org/10.1016/j.csr.2008.04.015.

Nilsen, F., Skogseth, R., Vaardal-Lunde, J., Inall, M., 2016. A simple shelf circulation model: intrusion of atlantic water on the west spitsbergen shelf. J. Phys. Oceanogr. 46 (4), 1209–1230. https://doi.org/10.1175/JPO-D-15-0058.1.

Nøttvedt, A., Livbjerg, F., Midbøe, P.S., Rasmussen, E., 1993. Hydrocarbon potential of the central spitsbergen basin. In: Vorren, T., Bergsager, E., Dahl-Stamnes, Ø.A., Holter, E., Johansen, B., Lie, E., Lund, T.B. (Eds.), Arctic Geology and Petroleum Potential. Norwegian Petroleum Society, Special Publication No. 2. Elsevier, pp. 333–361.

Parkinson, C.L., Cavalieri, D.A., 2012. Arctic sea ice variability and trends, 1979–2010 Cryosphere 6, 881–889. https://doi.org/10.5194/tc-6-881-2012.

Perovich, D., Meier, W., Tschudi, M., Farrell, S., Hendricks, S., Gerland, S., et al., 2018. Sea ice. In: Osborne, E., Richter-Menge, J., Jeffries, M. (Eds.). Arctic Report Card 2018. https://www.arctic.noaa.gov/Report-Card.

Roy, S., Senger, K., Braathen, A., Noormets, R., Hovland, M., Olaussen, S., 2014. Fluid migration pathways to seafloor seepage in inner Isfjorden and Adventfjorden, Svalbard. Norw. J. Geol. 94, 99–119.
Roy, S., Hovland, M., Noormets, R., Olaussen, S., 2015. Seepage in isfjorden and its tributary fjords, West Spitsbergen. Mar. Geol. 363, 146–159.
Roy, S., Hovland, M., Braathen, A., 2016. Evidence of fluid seepage in Grønfjorden, Spitsbergen: implications from an integrated acoustic study of seafloor morphology, marine sediments and tectonics. Mar. Geol. 380, 67–78.
Rutgers van der Loeff, M., Cassar, N., Nicolaus, M., Rabe, B., Stimac, I., 2014. The influence of sea-ice cover on air-sea gas exchange estimated with radon-222 profiles. J. Geophys. Res. Oceans 119.
Skogseth, R., Olivier, L.L.A., Nilsen, F., Falck, E., Fraser, N., Tverberg, V., Ledang, A.B., Vader, A., Jonassen, M.O., Søreide, J., Cottier, F., Berge, J., Ivanov, B.V., Falk-Petersen, S., 2020. Variability and decadal trends in the Isfjorden (Svalbard) ocean climate and circulation - an indicator for climate change in the European Arctic. Prog. Oceanogr. 187 https://doi.org/10.1016/j.pocean.2020.102394.
Stroeve, J.C., Serreze, M.C., Holland, M.M., Kay, J.E., Malanik, J., Barrett, A.P., 2012. The Arctic's rapidly shrinking sea ice cover: a research synthesis. Climatic Change 110, 1005–1027. https://doi.org/10.1007/s10584-011-0101-1.
Svendsen, H., Beszczynska-Møller, A., Hagen, J.O., Lefauconnier, B., Tverberg, V., Gerland, S., et al., 2002. The physical environment of Kongsfjorden-Krossfjorden, an Arctic fjord system in Svalbard. Polar Res. 21 (1), 133–166.
Silyakova, A., Jansson, P., Serov, P., Ferr_e, B., Pavlov, A.K., Hattermann, T., Niemann, H., 2020. Physical controls of dynamics of methane venting from a shallow seep area west of Svalbard. Continent. Shelf Res. 194, 104030.
Weslawski, J.M., Zajaczkowski, M., Szymelfenig, M., Keck, A., 1999. Influence of salinity and suspended matter on benthos of an Arctic tidal flat. ICES (Int. Counc. Explor. Sea) J. Mar. Sci. 56, 194e202.
Wiesenburg, D.A., Guinasso, N.L., 1979. Equilibrium solubilities of methane, carbon monoxide and hydrogen in water and seawater. J. Chem. A. Eng. Data 24 (1), 356–360.
Winkelmann, D., Knies, J., 2005. Recent distribution and accumulation of organic carbon on the continental margin west off Spitsbergen. G-cubed G^3. https://doi.org/10.1029/2005GC000916.
Zajaczkowski, M., Nygard, H., Nøst Hegseth, E., Berge, J., 2010. Vertical flux of particulate matter in an Arctic fjord: the case of lack of the sea-ice cover in Adventfjorden 2006–2007. Polar Biol. 33, 223–239. https://doi.org/10.1007/s00300-009-0699-x.